TGF-β Ligand Cross-Subfamily Interactions in the Response of *Caenorhabditis elegans* to Bacterial Pathogens

Emma Jo Ciccarelli[1,2], Zachary Wing[1], Moshe Bendelstein[1], Ramandeep Kaur Johal[1], Gurjot Singh[1], Ayelet Monas[1], Cathy Savage-Dunn[1,2*]

[1] Department of Biology, Queens College, CUNY, Flushing, NY

[2] PhD Program in Biology, The Graduate Center, CUNY, New York, NY

* Corresponding author

E-mail: cathy.savagedunn@qc.cuny.edu

Abstract

The Transforming Growth Factor beta (TGF-β) family consists of numerous secreted peptide growth factors that play significant roles in cell function, tissue patterning, and organismal homeostasis, including wound repair and immunity. Typically studied as homodimers, these ligands have the potential to diversify their functions through ligand interactions that are synergistic, cooperative, additive, and/or antagonistic. In the nematode *Caenorhabditis elegans*, there are only five TGF-β ligands, providing an opportunity to dissect ligand interactions in fewer combinations than in vertebrates. As in vertebrates, these ligands can be divided into bone morphogenetic protein (BMP) and TGF-β/Activin subfamilies that predominantly signal through discrete signaling pathways. The BMP subfamily ligand DBL-1 has been well studied for its role in the innate immune response in *C. elegans*. Here we show that all five TGF-β ligands play a role in the immune response. We also demonstrate that multiple TGF-β ligands act cooperatively as part of this response. We show that the two BMP-like ligands – DBL-1 and TIG-2 – function independently of each other in the immune response, while TIG-2/BMP and the TGF-β/Activin-like ligand TIG-3 function cooperatively. Structural modeling supports the potential for TIG-2 and TIG-3 to form heterodimers. Finally, we show that canonical DBL-1/BMP receptor and Smad signal transducers function in the response to bacterial pathogens, while components of the DAF-7 TGF-β/Activin signaling pathway do not play a role in survival. These results demonstrate a novel potential for BMP and TGF-β/Activin subfamily ligands to interact, and may provide a mechanism for distinguishing the developmental and homeostatic functions of these ligands from an acute response such as the innate immune response to bacterial pathogens.

Introduction

TGF-β signaling is a highly conserved mechanism that plays significant roles in development in organisms ranging from invertebrates to humans (Attisano and Wrana, 1996; Derynck *et al.,* 1998; Massagué *et al.*, 1998; Morita *et al.,* 2002). This signaling family also plays an important role in the post-developmental adult in maintaining homeostasis and repair (Massagué *et al.*, 1998; Blobe *et al.*, 2000; Massagué, 2000; Massagué, 2012), as well as serving as one of the highly conserved signaling mechanisms involved in the immune response (Medzhitov and Janeway, 1998; Hoffman *et al.,* 1999; Kim *et al.,* 2002; Schulenburg *et al.,* 2004; Millet and Ewbank, 2004; Irazoqui *et al.,* 2008; Partridge *et al.,* 2010). The canonical TGF-β family signaling cascade is initiated by binding of a dimerized ligand to a heterotetrametric receptor complex and mediated through activation of the Smad proteins to regulate transcription (Wrana *et al.*, 1994; Massagué *et al.*, 1998). The human genome contains 33 TGF-β ligands, seven type I receptors, and five type II receptors (Massagué *et al.*, 1998; Huminiecki *et al.*, 2009; Wrana, 2013; Aykul and Martinez-Hackert, 2016). Currently, active research is focused on the mechanisms that mediate specific or promiscuous interactions between ligands and receptors, and the consequences for Smad signaling. These mechanisms have profound implications for normal development and disease (Silberstein and Daniel, 1987; Akhurst and Derynck, 2001; Li *et al.,* 2006; Massagué *et al.*, 2008; Pohlers *et al.,* 2009; Zamarron and Chen, 20011; Principe *et al.,* 2014). The number of potential interactions, however, increases the difficulty of these analyses. The reduced repertoire of ligands and receptors in invertebrate organisms provides an opportunity to study ligand-receptor functional interactions more completely. Due to the conservation of TGF-β signaling pathways, studies in the genetically tractable organisms

66 Drosophila and *C. elegans* have resulted in universal insights into conserved signaling
67 mechanisms.
68
69 In *C. elegans*, there are five ligands associated with TGF- β signaling: DBL-1, DAF-7, TIG-2,
70 TIG-3, and UNC-129. DAF-7 and TIG-3 are most appropriately classified as TGF-β/Activin-like
71 ligands, whereas DBL-1 and TIG-2 share the most similarity with BMP ligands in mammals
72 (Harpin, 2004; Patterson and Padgett, 2000). Of the five TGF-β ligands in *C. elegans*, only two
73 have well-characterized signaling pathways through which they signal (Patterson and Padgett,
74 2000; MacNeill *et al.,* 2009). The TGF-β-like ligand DAF-7 is the regulator of the dauer pathway
75 and its expression in favorable conditions prevents entry into the dauer larval stage (Ren *et al.,*
76 1996; Schackwitz *et al.,* 1996; Inoue and Thomas, 2000). The BMP-like ligand DBL-1 activates
77 the BMP-like pathway in the worm and plays a significant role in development (Suzuki *et al.,*
78 1999; Yoshida *et al.,* 2001; Wang *et al.,* 2002). UNC-129, TIG-2, and TIG-3 have been
79 classified (as BMP-like or TGF-β-like) based on their structural characteristics, but have not
80 been fully associated with all members of either the BMP-like or TGF-β-like signaling pathways
81 in *C. elegans* (Harpin, 2004; Patterson and Padgett, 2000).
82
83 Previous work from our lab and others has demonstrated that the BMP homolog DBL-1
84 functions in the innate immune response of *C. elegans* to pathogenic bacteria and fungi by
85 inducing the expression of antimicrobial peptide genes in response to pathogen exposure.
86 (Ciccarelli *et al.*, 2023; Mallo *et al.,* 2002; Zugasti and Ewbank, 2009; Zhang and Zhang, 2012).
87 Here we demonstrate that the DBL-1 ligand is only one of four TGF-β family ligands with a
88 significant and consistent role in the immune response to two gram-negative bacterial pathogens.

89 We show that in response to either *Serratia marcescens* or *Photorhabdus luminescens*, multiple
90 TGF-β family ligand mutants have a significant reduction in survival compared to control
91 animals. We also demonstrate that two BMP-like ligands, DBL-1 and TIG-2, act independently
92 of each other. In contrast, we have shown a non-additive relationship between TIG-2/BMP and
93 the TGF-β-like ligand TIG-3, suggesting a cooperative role for these two distinct ligands in the
94 immune response. Finally, we have identified signaling components with similar phenotypes to
95 TIG-2 and TIG-3 in response to bacterial pathogen. Our studies thus uncover novel signaling
96 paradigms that may act more broadly to distinguish distinct physiological outcomes regulated by
97 TGF-β ligands.
98

99 **Materials and Methods**

100 **Nematode Strains and Growth Conditions**

101 *C. elegans* were maintained on *E. coli* (DA837) using EZ worm plates containing streptomycin.
102 Worms were maintained at 20ºC, except in experiments using dauer pathway mutants. These
103 strains were maintained at 15ºC to prevent entry into dauer. The N2 strain is used as a control.
104 All strains used in this study are: N2, *daf-1(m40), daf-7(m62), daf-8(e1398), daf-14(m77),*
105 *sma-2(e502), sma-3(wk30), sma-4(jj278), sma-6(wk7), tig-2(ok3336)*, *tig-2(ok3416),*
106 *tig-3(tm2092)*, *unc-129(ev554), daf-7(m62);dbl-1(wk70), tig-2(ok3416)dbl-1(wk70),*
107 *tig-2(ok3416);unc-129(ev554), tig-3(tm2092);tig-2(ok3416), tig-3(tm2092);unc-129(ev554),*
108 *tig-3(tm2092);tig-2(ok3416);unc-129(ev554), pdbl-1*::GFP.
109

110 **Bacteria**

111 Control bacteria in all experiments is *E. coli* strain DA837, cultured at 37ºC. *S. marcescens* strain
112 Db11 (cultured at 37ºC) and *P. luminescens* (cultured at 30ºC) were used for bacterial pathogen
113 in survival analyses. *S. marcescens* (Db11) is seeded on EZ worm plates containing streptomycin
114 and grown overnight at 37ºC. *P. luminescens* is seeded on EZ worm plates with no antibiotic and
115 grown overnight at 30ºC.
116
117 **Survival Analysis**
118 Survival plates were prepared at least one day prior to use. Each plate was seeded with 500µl
119 pathogenic bacteria in a full lawn. FuDR, at a concentration of 50 µM per plate, was used to
120 prevent reproduction and reduce the incidence of matricide during survival analysis. Survivals
121 were conducted at 20ºC, except survivals using dauer pathway mutants, which were conducted at
122 15ºC to minimize dauer entry (unless otherwise stated). Survival analyses were repeated for all
123 ligand experiments and DBL-1 pathway experiments. All graphs made using GraphPad Prism
124 and statistical analysis performed using Logrank/Mantel Cox test.
125
126 **Fluorescence Imaging**
127 Fluorescence imaging of the *dbl-1p*::GFP transcriptional reporter strain was done using a Zeiss
128 ApoTome with AxioVision software and a (20X) objective. Exposure times were kept consistent.
129 Image analysis and fluorescence intensity measurements were done using ImageJ software.
130 Fluorescence intensity was measured for ten nuclei in each of four worms per bacterial exposure
131 condition.
132
133 **qRT-PCR Analysis**

134 qRT-PCR analysis was performed on collected samples of N2 control animals with or without
135 24-hour *P. luminescens* pathogen exposure. RNA was obtained by a previously described
136 protocol (Yin *et al.*, 2015) and followed by use of the Qiagen RNeasy miniprep kit (Cat. No.
137 74104). cDNA was made using SuperScript IV VILO Master Mix (Cat. No.11756050) from
138 Invitrogen, Waltham, MA. qRT-PCR analysis was done using Power SYBR Green PCR Master
139 Mix (Cat. No. 4367659) from Applied Biosystems, Waltham, MA. qRT-PCR was repeated on
140 separate biological replicates. Delta delta Ct analysis was done using Applied Biosystems and
141 StepOne software. Graphs made using GraphPad Prism software.
142

143 **Structural Modeling**

144 SignalP 6.0 was used to predict the signal sequence for TGF-β family members. No signal
145 sequence for TIG-3 isoform A could be determined, and this potential isoform was not
146 considered further. For TIG-3 isoform B, the prodomain and mature domain are defined using a
147 consensus cleavage site (Newfeld and Wisotzkey, 2020). The TIG-2 cleavage site was
148 determined by manual sequence analysis using the (R/K)-X_n-(R/K) motif as a reference where X
149 is an amino acid sequence of length n such that n is even and $0 \leq n \leq 6$ (Hinck *et al.*, 2016). The
150 existence of multiple functional cleavage sites is common (Hinck *et al.*, 2016), and two such
151 sites (RSRR and KVKR) were identified. Both cleavage sites are supported by structural
152 modeling and preserve the cystine knot domain. The main distinction between the two sites is the
153 length of the initial disordered region of the mature ligand (RSRR: 134-residue vs. KVKR: 116-
154 residue mature form). Previously reported cleavage sites were used for the remaining TGF-β
155 family members (Hinck *et al.*, 2016). The full-length domain (Fig. 7C) is defined as the entire
156 monomer sequence, excluding the signal sequence. Dimeric structures were modeled using the

157 ColabFold (version 1.5.2) implementation of AlphaFold2-multimer (version 3). The
158 AlphaFold2_mmseqs2 notebook was run under the default settings, and amber relaxation was
159 applied to all five structural models. The model assigned rank one was selected for visualization
160 and analysis. Interchain residue contacts (Fig. 6, Fig. 7C) within 4 Å and their predicted aligned
161 error (PAE) value were identified using UCSF ChimeraX (version 1.5). One-dimensional amino
162 acid sequence tracks (Fig. 6) include only dimer-interface residues that are within a distance of 4
163 Å and have a low positional error (PAE < 5 Å). Images of three-dimensional structures were
164 rendered using PyMOL (version 2.5.4). pLDDT color coding and secondary structure annotation
165 of one-dimensional amino acid sequences were generated using iCn3D (version 3.24.2) and
166 reformatted. The alpha helices used in secondary structure labeling are modified vectors from
167 BioRender.com.
168

169 **Results**

170 **The BMP-like Ligands DBL-1 and TIG-2 are Independently Required for *C. elegans***
171 **Survival on Bacterial Pathogen**

172 *C. elegans* has five TGF-β like ligands: DBL-1, DAF-7, UNC-129, TIG-2, and TIG-3. It is
173 established that loss of DBL-1, one of two BMP-like ligands in *C. elegans*, results in reduced
174 survival of animals on bacterial pathogen (Ciccarelli *et al.,* 2023; Mallo, 2002). In a variety of
175 physiological contexts, heterodimers of BMP ligands are functionally required or outperform
176 homodimers (Tillet *et al*., 2018; Little and Mullins, 2009; Kim *et al.*, 2019; Shimmi *et al.,* 2005).
177 We therefore considered the possibility that DBL-1/BMP functions with the other BMP-like
178 ligand in the worm, TIG-2. The DBL-1 pathway has been thoroughly studied in response to
179 exposure to the gram-negative bacterium *Serratia marcescens*, where the worm's survival is

180 significantly hindered by gut colonization as a consequence of the pathogen supplanting the
181 normal bacterial food source (Mallo, 2002). To test the role of TIG-2/BMP, we quantified
182 survival of two *tig-2* mutant strains on *S. marcescens* and compared these survival rates to *dbl-1*
183 and N2 (wild type) control. We used *tig-2(ok3336),* a 500 bp deletion allele, and *tig-2(ok3416),*
184 an 800 bp deletion allele, and found that both *tig-2* mutant strains resulted in reduced survival
185 against bacterial infection (Fig. 1A). Survival rates for both *tig-2* mutant strains were
186 significantly different compared to control. The larger deletion allele resulted in a survival defect
187 similar to that of *dbl-1* mutants and more pronounced than the survival defect caused by the 500
188 bp deletion. We further tested the effect of mutating *tig-2* on immunity by analyzing the survival
189 of *tig-2* mutant animals on the more virulent *P. luminescens* bacteria. We found that *tig-2*
190 mutants survived significantly worse than control animals (Fig. 1B). Interestingly, we found that
191 *tig-2* mutants had an even more pronounced susceptibility to *P. luminescens* infection than *dbl-1*
192 mutants, suggesting a more significant role for TIG-2 in response to *P. luminescens* infection.
193
194 Given that both BMP ligands function in the *C. elegans* immune response, we next considered
195 whether they act independently or together by determining the phenotype of double mutants. If
196 these ligands act independently, then we expect the double mutant to have a more severe
197 phenotype than the single mutants, reflecting the disruption of two independent pathways. If they
198 act together, such as in a heterodimer, then we expect the double mutant to have the same
199 phenotype as the single mutants due to the failure of individual ligands to provide physiological
200 function. When grown on *P. luminescens*, *tig-2dbl-1* double mutant animals demonstrated a
201 more pronounced reduction in survival compared to either the *tig-2* or *dbl-1* single mutant
202 animals (Fig. 1C). Our survival analysis shows an additive effect of these two mutations

203 combined. These results indicate that the two BMP-like ligands – DBL-1 and TIG-2 – act
204 independently of each other in the response to *P. luminescens*.
205
206 At the time of these experiments, no phenotype had been reported for *tig-2* mutants, so we were
207 encouraged to have identified a biological function for this ligand. To rule out a general effect on
208 lifespan, we followed our survival analysis with a lifespan on control *E. coli* bacteria. Both *tig-2*
209 mutants displayed a lifespan similar to control animals (Fig. S1). Animals mutant for *dbl-1* also
210 had an unaffected lifespan on control bacteria, as expected. These results indicate that the
211 reduced survival of *tig-2* on bacterial pathogen is specific to its susceptibility to infection and not
212 reflective of a lifespan phenotype. Together these results demonstrate significant roles for the
213 two BMP-like ligands – DBL-1 and TIG-2 – in the response to pathogenic bacterial infection,
214 although independent of each other.

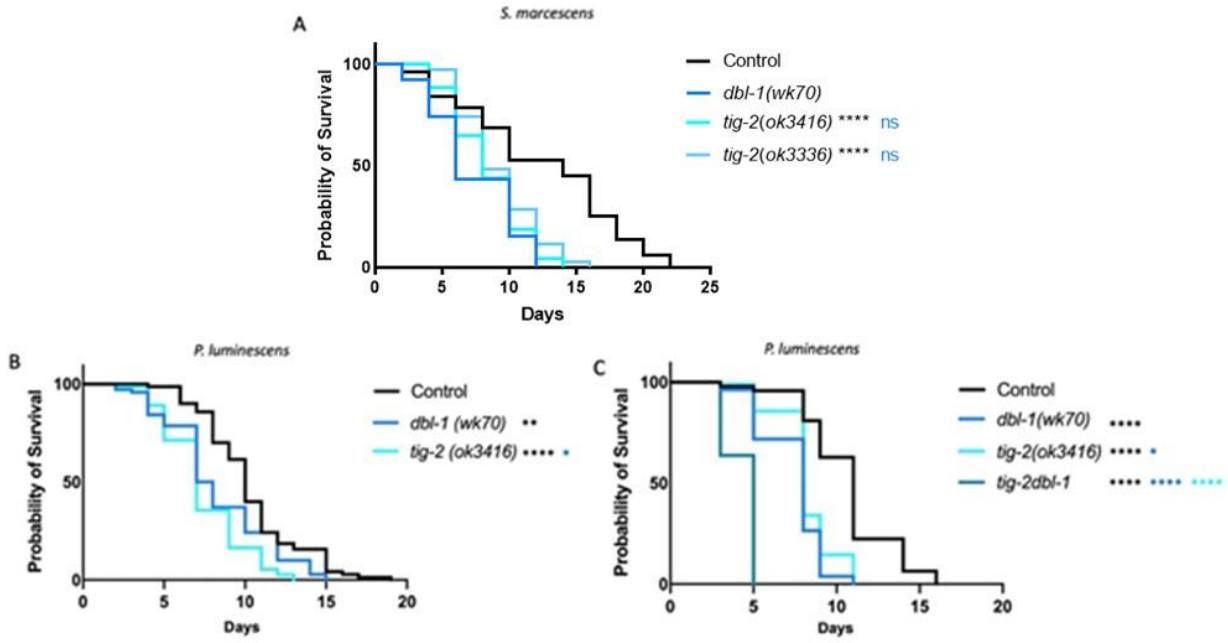

Figure 1. The BMP-like Ligands DBL-1 and TIG-2 are Required for *C. elegans* Survival on Bacterial Pathogen.

A. Survival analysis of *dbl-1(wk70)* and two *tig-2* mutants (*tig-2(ok3416)* and *(tig-2(ok3336)*) on *S. marcescens* bacteria. *n* values: Control (51), *dbl-1* (39), *tig-2* (43), *tig*-2 (35). **B.** Survival analysis of *dbl-1(wk70)* and *tig-2(ok3416)* on *P. luminescens* bacteria. *n* values: Control (70), *dbl-1* (70), *tig-2* (73). **C.** Survival analysis of *tig-2dbl-1* double mutant on *P. luminescens. n* values: Control (94), *dbl-1* (53), *tig-2* (97), *tig-2dbl-1* (55). Statistical analysis done using Log-rank (Mantel-Cox) Test. ns $p > 0.05$; * $p \leq 0.05$; ** $p \leq 0.01$; **** $p < 0.0001$. Black asterisks denote significance relative to control, blue is significance relative to *dbl-1*, and teal is significance relative to *tig-2.*

227 **Five TGF-β Ligands Demonstrate Involvement in Survival Against Bacterial Infection**

228 We next were interested in determining if the remaining TGF-β ligands – DAF-7, UNC-129, and
229 TIG-3 – play a role in the *C. elegans* immune response. UNC-129 and TIG-3 are "orphan"
230 ligands without known receptors and signaling components. DAF-7 is well characterized as the
231 ligand in the dauer pathway, and *daf-7* mutants demonstrate a high incidence of dauer when
232 grown at 20ºC. For this reason, the strains analyzed alongside *daf-7* were all grown to the fourth
233 larval stage (L4) at 15ºC and shifted to 20ºC when moved to pathogen plates.

234

235 We found that in mutants of any of the five TGF-β ligands, survival against pathogenic *P.*
236 *luminescens* infection is significantly reduced, with variability between trials for some ligands
237 (Fig. 2A and Fig. 2B). In particular, *unc-129* mutants have variable survival outcomes.
238 Surprisingly, *dbl-1* mutant animals also have a variable survival pattern on *P. luminescens*, in
239 spite of their well-characterized susceptibility to a variety of bacterial and fungal pathogens. In
240 contrast, TIG-2, TIG-3, and DAF-7 show consistently significant susceptibility in response to *P.*
241 *luminescens*, concordant with the hypothesis that distinct signaling mechanisms are responsible
242 for the specific responses against different bacterial pathogens.

243

244 To determine whether expression of any of these ligands is induced in response to pathogen, we
245 used qRT-PCR to evaluate expression levels of genes encoding TGF-β ligands in wild-type
246 animals. Upon 24-hour exposure to *P. luminescens* bacteria, the relative expression of all five
247 TGF-β ligand genes demonstrated no significant alteration compared to control conditions (Fig.
248 2C). Additionally, analysis of a *dbl-1* transcriptional reporter showed no change in fluorescence
249 levels on pathogen compared to control bacteria (Fig. S2). We conclude that although these

250 ligands function in response to pathogen, they are not subject to widespread transcriptional

251 induction.

252

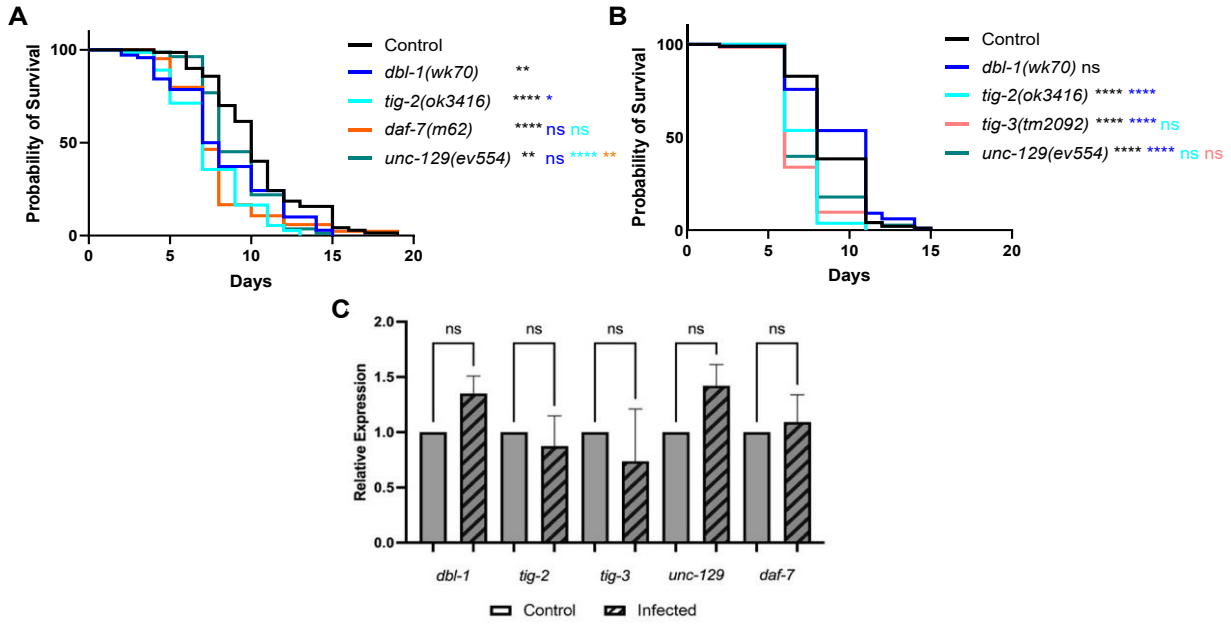

Figure 2. Five TGF-β Ligands Demonstrate Involvement in Survival Against Bacterial Infection.

A. Survival of TGF-β ligand mutants on *P. luminescens* bacteria. For this trial, strains were grown at 15°C to avoid dauer formation by *daf-7* mutants and shifted to 20°C at L4 when exposed to pathogen. *n* values: Control (70), *dbl-1* (70), *tig-2* (73), *daf-7* (84), *unc-129* (82). **B.** Survival of TGF-β ligand mutants on *P. luminescens* bacteria. n values: Control (99), *dbl-1* (99), *tig-2* (108), *tig-3* (62), *unc-129* (73). **C.** qRT-PCR analysis showing relative expression of TGF-β ligand genes upon 24-hour exposure to *P. luminescens* in Control animals. qRT-PCR data represents repeated analyses of two biological replicates. Statistical analysis done using One-way ANOVA with multiple comparison test. For survivals, statistical analysis done using Log-rank (Mantel-Cox) Test. ns $p > 0.05$; * $p \leq 0.05$; ** $p \leq 0.01$; **** $p < 0.0001$. Black asterisks denote significance relative to control, blue is significance relative to *dbl-1,* teal is significance relative to *tig-2,* orange is significance relative to *daf-7*, and salmon is significance relative to *tig-3.*

268 **Multiple TGF-β Ligand Pairs Demonstrate Cooperative Interaction in the *C. elegans***
269 **Response to Bacterial Infection**

270 We next looked for interactions between the remaining *C. elegans* TGF-β ligands upon exposure
271 to bacterial infection by testing double mutants as previously described for *tig-2dbl-1*. We
272 analyzed the *tig-3;tig-2* double mutant, deficient in both the BMP-like ligand TIG-2 and the
273 TGF-β/Activin-like ligand TIG-3, for survival on *P. luminescens*. We found that when grown on
274 bacterial pathogen, the *tig-3;tig-2* double mutants demonstrated a survival pattern not
275 significantly different from either the *tig-2* or the *tig-3* single mutants (Fig. 3A). This result
276 contrasts with our analysis of the BMP-like ligands DBL-1 and TIG-2, and suggests that
277 TIG-2/BMP and TIG-3/(TGF-β/Activin) are acting in the immune response in a cooperative
278 manner.
279

280 We also assessed the survival pattern of *daf-7;dbl-1* double mutants on pathogenic bacteria. For
281 this experiment, animals were grown at 15ºC to minimize dauer entry in *daf-7* mutants. Survival
282 of *daf-7;dbl-1* double mutants was not significantly different compared to *dbl-1* single mutants
283 (Fig. 3B). The survival pattern of *daf-7;dbl-1* double mutant animals indicates a potential
284 relationship in which both ligands function in a single pathway. This cooperativity is intriguing
285 as the BMP-like ligand DBL-1 is known to signal through a different Type I receptor and
286 different Smads than the TGF-β/Activin-like ligand DAF-7.
287

288 Finally, we compared the survival pattern of double and triple mutants for *unc-129*. Although
289 *unc-129* mutants have weak and variable effects on survival, the *unc-129* gene did show some
290 potential interactions with other ligand genes. Survival of *unc-129;tig-2* double mutants are not

291 significantly different from *tig-2* single mutants (Fig. S1). In contrast, in *tig-3;unc-129* double
292 mutants, the decreased survival of *tig-3* mutants is suppressed (Fig. S2), suggesting a potential
293 antagonistic interaction between UNC-129 and TIG-3. Overall, our results from these survival
294 analyses indicate a complex relationship between the TGF-β family ligands in the immune
295 response. Most surprisingly, ligands that demonstrate cooperative relationships are those from
296 different classes of TGF-β ligands – BMP-like TIG-2 with TGF-β/Activin-like TIG-2; and
297 possibly BMP-like DBL-1 with TGF-β/Activin-like DAF-7.
298

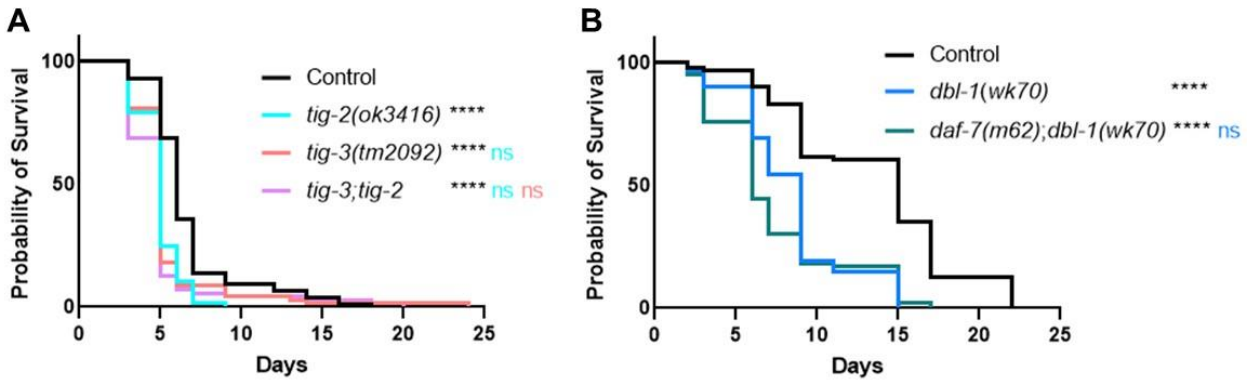

Figure 3. Multiple TGF-β Ligands Demonstrate Cooperative Interaction in the *C. elegans* Response to Bacterial Infection.

A. Survival analysis of *tig-3(tm2092);tig-2(ok3416)* double mutants on *P. luminescens* bacteria. *n* values: Control (73), *tig-2* (68), *tig-3* (67), *tig-3;tig-2* (71). **B.** Survival analysis of *daf-7(m62);dbl-1(wk70)* double mutants on *P. luminescens* bacteria. *n* values: Control (94), *dbl-1* (94), *daf-7* (83). For this trial, strains were grown at 15ºC to avoid dauer formation by *daf-7* mutants and shifted to 20ºC at L4 when exposed to pathogen. Statistical analysis done using Log-rank (Mantel-Cox) Test. ns $p > 0.05$; **** $p < 0.0001$. Black asterisks show significance relative to control, blue is significance relative to *dbl-1,* teal is significance relative to *tig-2*, and salmon is significance relative to *tig-3.*

310 **Canonical BMP Signaling Components are Involved in the *C. elegans* Immune Response**

311 The two TGF-β pathways in *C. elegans* are known to signal through canonical mechanisms upon
312 activation. DBL-1 signals through the BMP-like pathway with ligand binding to the single Type
313 II receptor DAF-4 and the Type I receptor SMA-6. The BMP pathway Smads – SMA-2, SMA-3,
314 and SMA-4 – transduce the intracellular signal allowing for gene regulation. The TGF-β/Activin-
315 like ligand DAF-7 signals through the TGF-β/Activin-like pathway components, including the
316 Type I receptor DAF-1 and the Smads DAF-8, DAF-14, and DAF-3 (Estevez *et al.*, 1993;
317 Savage *et al.*, 1996; Suzuki *et al.*, 1999; Krishna *et al.*, 1999; Savage-Dunn and Padgett, 2017).
318 Both pathways converge on the single Type II receptor DAF-4. Previous work has shown that in
319 response to fungal infection of the hypodermis, DBL-1 signals in a pathway utilizing only one
320 receptor-regulated Smad (R-Smad SMA-3) without its typical partner R-Smad SMA-2 or the Co-
321 Smad SMA-4 (Zugasti and Ewbank, 2009). Signaling without a Co-Smad is considered non-
322 canonical. We were therefore interested in which components of the BMP-like and
323 TGF-β/Activin-like pathways are required during bacterial infection and whether non-canonical
324 mechanisms are invoked.

325

326 Our survival analysis of DBL-1 pathway components shows a consistently reduced survival
327 pattern for R-Smad mutants *sma-2* and *sma-3* as well as for Co-Smad mutant *sma-4* (Fig. 4A).
328 This result is consistent with a significant role for the BMP pathway Smads in the *C. elegans*
329 response to bacterial pathogen, unlike the results previously shown on fungal infection. Survival
330 analysis of BMP pathway receptors showed a reduced survival pattern for the BMP Type I
331 receptor mutant *sma-6* (Fig. 4B). We observe consistently reduced survival for *sma-6* mutants,
332 with slight variability in the significance of the survival rate across trials.

333

334 We analyzed the survival patterns of the DAF-7 pathway mutants grown at 15ºC on *P.*
335 *luminescens* bacteria and found either no phenotype or a mild survival deficit. In particular, R-
336 Smad mutant *daf-8* demonstrated a slightly reduced rate of survival (Fig. 4C), while neither R-
337 Smad mutant *daf-14* (Fig. 4C) nor Type I receptor *daf-1*(Fig. 4D) had significantly altered
338 survival compared to control animals. Thus, although TGF-β/Activin-like ligands DAF-7 and
339 TIG-3 play a role in the immune response against bacterial pathogen, they are unlikely to signal
340 through the canonical TGF-β/Activin signaling components.

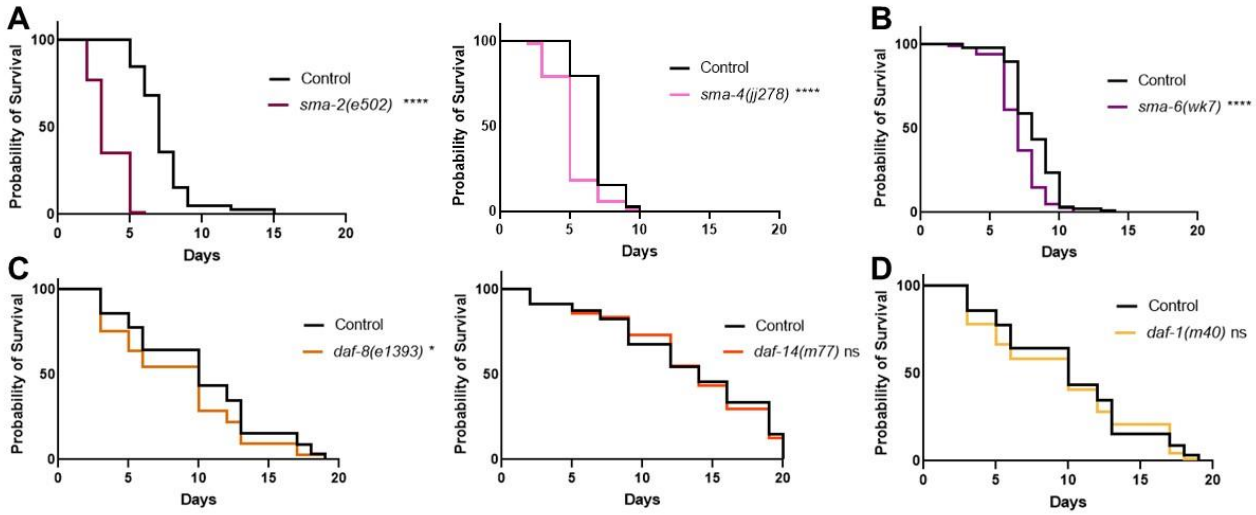

Figure 4. Canonical BMP Signaling Components are Involved in the *C. elegans* Immune Response.

A. Survival of DBL-1 R-Smad mutant *sma-2(e502)* and Co-Smad mutant *sma-4(jj278)* on *P. luminescens* bacteria. *n* values: Control (103), *sma-2* (88), Control (78), *sma-4* (72). **B.** Survival analysis of Type I receptor *sma-6(wk7)* on *P. luminescens*. *n* values: Control (88), *sma-6* (100). **C.** Survival of DAF-7 pathway R-Smad mutants *daf-8(e1393)* and *daf-14(m77)* on *P. luminescens* bacteria. *n* values: Control (90), *daf-8* (77), Control (81), *daf-14* (78). **D.** Survival analysis of Type I receptor *daf-1(m40)* on *P. luminescens*. *n* values: Control (90), *daf-1* (86). Statistical analysis done using Log-rank (Mantel-Cox) Test. ns $p > 0.05$; * $p \leq 0.05$; **** $p < 0.0001$.

352 ***tig-2* and *tig-3* Animals Share Reduced Survival and Pumping Rate Phenotypes with *sma-3***
353 **Mutants**

354 Thus far, we have shown that TIG-2 (BMP) and TIG-3 (TGF-β/Activin) play more significant
355 roles in survival on *P. luminescens* bacteria than DBL-1/BMP, and that BMP signaling
356 components play a more significant role than TGF-β/Activin signaling components. These
357 observations suggest a model in which TIG-2 and TIG-3 signal through components previously
358 presumed to respond to DBL-1. To test this model, we compared *tig-2* and *tig-3* phenotypes with
359 those of *sma-3* and *dbl-1.* Survival analysis directly comparing *dbl-1* and *sma-3* mutants on *P.*
360 *luminescens* demonstrates that while both strains have a decreased survival pattern as compared
361 to control, *sma-3* mutants have a significantly reduced survival rate compared to *dbl-1* mutants
362 (Fig. 5A), suggesting that SMA-3 is responding to other signaling ligands instead of or in
363 addition to DBL-1. Notably, *tig-2* and *tig-3* survival phenotypes are highly similar to those of
364 *sma-3* mutants (Fig. 5B), consistent with a model in which TIG-2 and TIG-3 signal through R-
365 Smad SMA-3 in response to *P. luminescens* pathogen.
366

367 To test this model further, we analyzed an additional phenotype associated with response to *P.*
368 *luminescens*, reduced pharyngeal pumping rate (Ciccarelli *et al.,* 2023). Pharyngeal pumping rate
369 analysis revealed *sma-3*, but not *dbl-1*, mutants have a significant reduction in pharyngeal
370 pumping rate, and this reduction is indistinguishable from that of *tig-2* and *tig-3* mutants, as well
371 as of the *tig-3;tig-2* double mutant (Fig. 5C-D). This similarity further strengthens the model that
372 TIG-2 and TIG-3 signal through SMA-3 in this context.
373

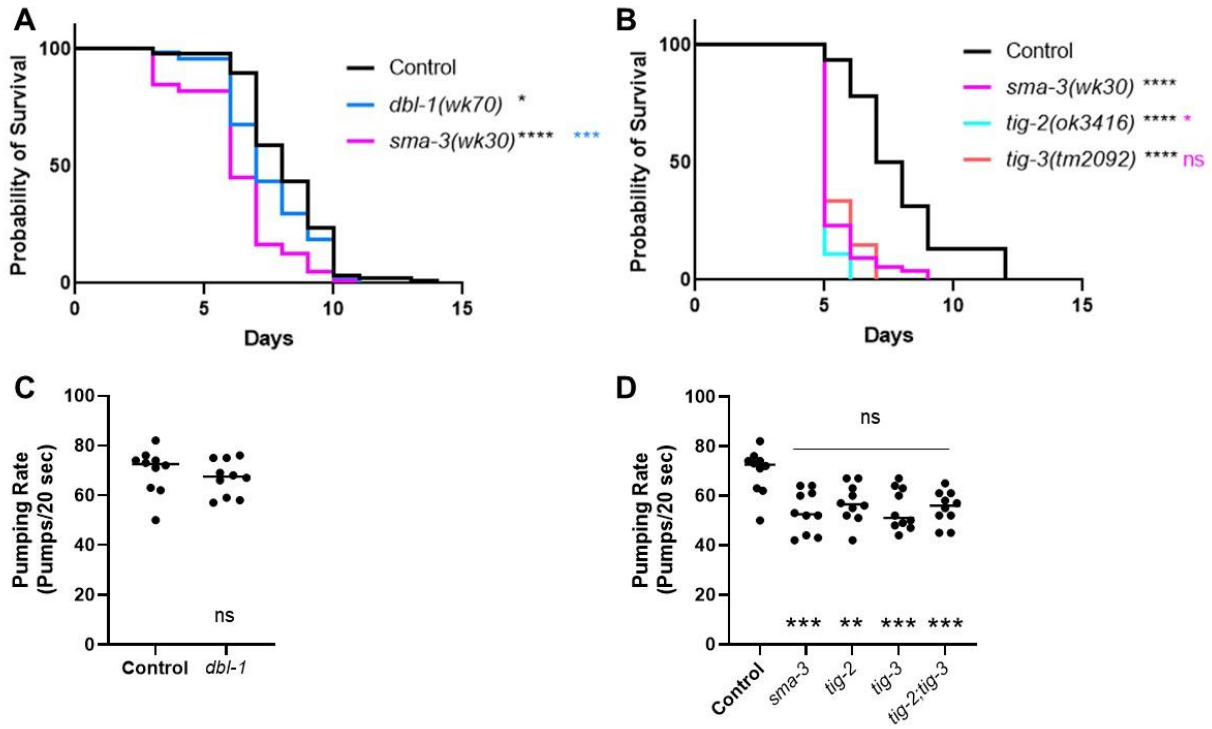

Figure 5. *tig-2* and *tig-3* Animals Share Reduced Survival and Pumping Rate Phenotypes with *sma-3* Mutants.

A. Survival of *dbl-1(wk70)* and *sma-3(wk30)*. n values: Control (88), *dbl-1* (74), *sma-3* (78). Black asterisks are compared to control. Blue asterisks are compared to *dbl-1*. **B.** Survival of *sma-3(wk30)* mutants compared to *tig-2(ok3416)* and *tig-3(tm2092)*. Black asterisks are compared to control. Pink asterisks are compared to *sma-3*. *n* values: Control (92), *sma-3* (74), *tig-2* (55), *tig-3* (54). Statistical analysis for all survivals done using Log-rank (Mantel-Cox) test. Survivals were repeated. **C.** Pumping rate per 20 seconds for *dbl-1(wk70)* compared to Control. Statistical analysis done using t test. **D.** Pumping rate per 20 seconds for *sma-3(wk30), tig-2(ok3416), tig-3(tm2092),* and *tig-3;tig-2*. Black asterisks are compared to Control. Pink asterisks are compared to *sma-3*. Statistical analysis done using One-way ANOVA with Multiple Comparison Test. *n* values for all pumping rate experiments: ten worms per strain. Pumping rate

387 experiments were repeated on independent biological samples. ns $p > 0.05$; * $p \leq 0.05$; ** $p \leq$

388 0.01; *** $p \leq 0.001$; **** $p < 0.0001$.

389 **Structural Modeling of Potential Protein-Protein Interaction Between TIG-2/BMP and**
390 **TIG-3/(TGF-β/Activin)**

391 The cooperative action observed between TIG-2/BMP and TIG-3/(TGF-β/Activin) in the *C.*
392 *elegans* immune response could be evidence of TIG-2/TIG-3 heterodimers. Alternatively,
393 homodimers of TIG-2 and of TIG-3 could act together through a receptor clustering mechanism
394 (Ramachandran *et al*., 2018). To determine whether heterodimers of TIG-2 and TIG-3 are
395 feasible, we performed structural modeling *in silico.* Using the ColabFold (Mirdita *et al*., 2022)
396 implementation of AlphaFold2 (Jumper *et al*., 2021), we asked whether confident structural
397 predictions could be made for TIG-2 homodimers, TIG-3 homodimers, and TIG-2/TIG-3
398 heterodimers. We first analyzed interactions between mature bioactive domains, using consensus
399 proteolytical cleavage sites (see Materials and Methods). Using the mature domain of TIG-2, we
400 were able to generate a strongly supported model for the TIG-2 homodimer that recapitulates the
401 well-known "butterfly" structure of TGF-β family ligand dimers (Fig. 6). In contrast, the
402 potential for the TIG-3 mature bioactive domain to form homodimers was not supported by
403 ColabFold, with a poor interface predicted template modeling (ipTM) score of 0.288. Using
404 TIG-2 and TIG-3 for modeling, however, resulted in a heterodimer with a high ipTM score of
405 0.783, similar to that of the TIG-2 homodimer (0.875), as well as to those of known heterodimers
406 (Fig. S6). Intriguingly, both TIG-2 and TIG-3 lack the conserved cysteine residue that mediates
407 interchain disulfide bridges in most TGF-β family ligands (Fig. S4). Two other TGF-β family
408 members that also lack these cysteines are BMP15 and GDF9 (Mottershead *et al.,* 2015). These
409 ligands form stable homo- and heterodimers without interchain disulfide bridges. In fact,
410 GDF9/BMP15 heterodimers, known as cumulin, are capable of forming from homodimers by
411 subunit exchange (Mottershead *et al.,* 2015).

412 In vivo, prodomains present in the uncleaved precursors have been shown to be required for
413 heterodimer formation between BMP4 and BMP7 (Neugebauer *et al.,* 2015). We therefore
414 performed structural modeling with full-length proteins (prodomain + mature domain). In these
415 models, additional potential contacts between TIG-2 and TIG-3 are identified (Fig. 7). The
416 TIG-2/TIG-2 procomplex resembles a BMP dimer with the prodomains remaining separate from
417 each other, but making contacts with the mature domains (Fig. 7A, C). In the TIG-2/TIG-3
418 predicted procomplex, the TIG-3 prodomain makes contact with the TIG-2 prodomain and
419 mature domain (Fig. 7B, C). Thus, structural modeling of the full-length proteins also supports
420 the possibility of heterodimer formation consistent with our functional genetic analysis. This
421 model can now be tested with biochemical analysis of protein-protein interactions.
422

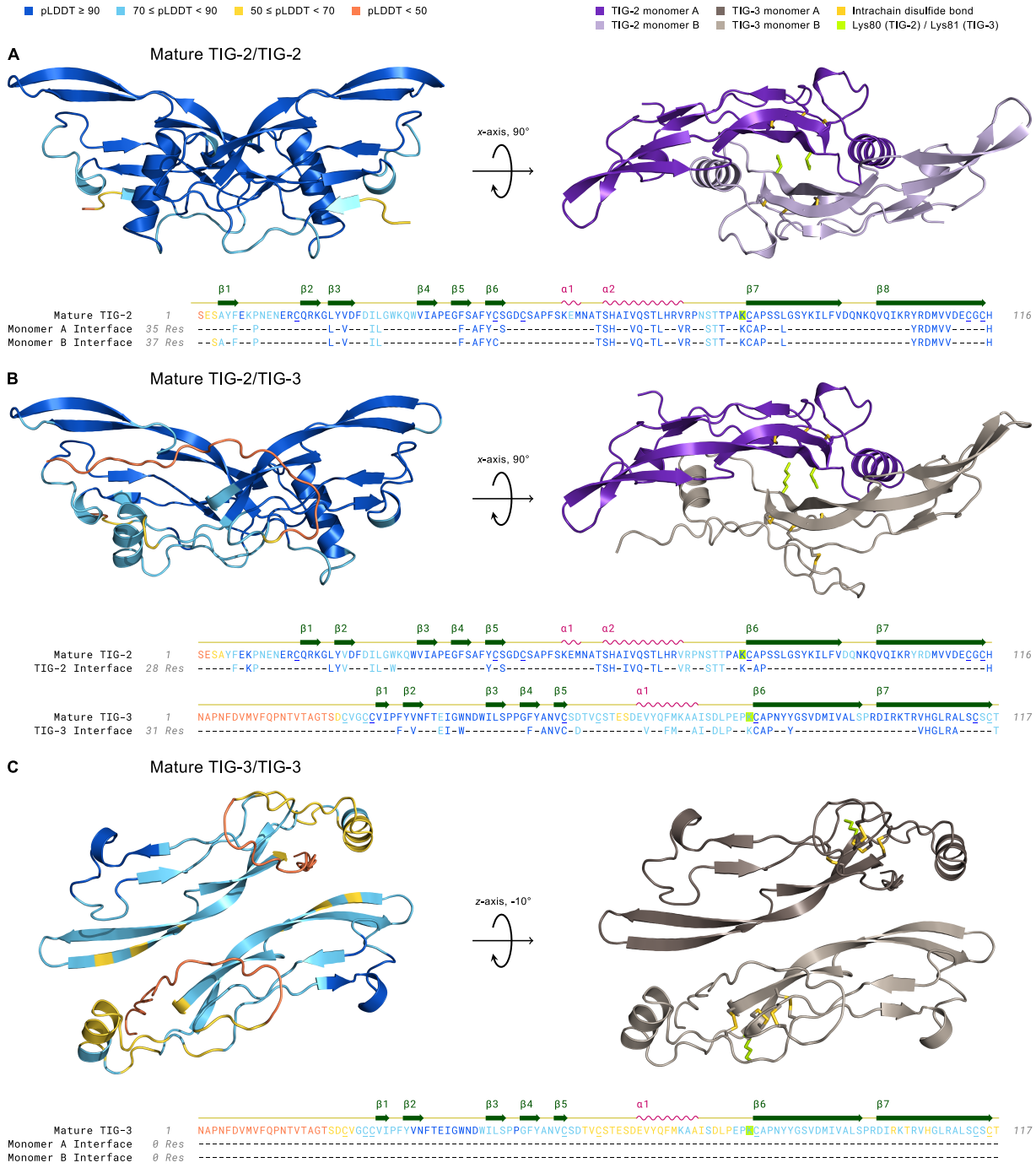

Figure 6. Structural Modeling of TIG-2 and TIG-3 Mature Ligand Homo- and Heterodimer Complexes Using AlphaFold2. Left complex: 3D structures are colored by pLDDT confidence score with deep blue corresponding to regions of very high confidence and orange representing regions of very low confidence or disorder. Right complex: The mature

429 dimer as in the left panel, but colored by monomer and following geometric rotation. All
430 cysteine residues (underlined) in mature TIG-2 (with 15-81, 44-113, 48-115 disulfides) and TIG-
431 3 (with 22-26, 25-82, 54-114, 59-116 disulfides) homo- and heterodimers are paired in intrachain
432 disulfide bonds (gold) within the cystine knot domain. The cysteine residue that forms the
433 interchain disulfide bond in the mature dimer is absent in TIG-2 and TIG-3, similar to GDF-3,
434 GDF-9, and BMP-15 (Hinck *et al.*, 2016). Interestingly, lysine (yellow-green), with its reactive
435 ε-amino group upon deprotonation, is instead substituted for this cysteine residue in both TIG-2
436 (Lys80) and TIG-3 (Lys81). Amino Acid Sequence: Residues are colored by pLDDT score. The
437 monomer interface tracks consist of confidently-predicted dimer-interface contacts (see
438 Methods). A. Mature TIG-2(purple)/TIG-2(lavender) exhibits high confidence with respect to
439 per-residue structural modeling (pLDDT: 92.7), pairwise residue alignment confidence (pTM:
440 0.868), and dimeric interaction confidence (ipTM: 0.875). B. Mature TIG-2(purple)/TIG-3(gray-
441 beige) is confidently modeled regarding its structure and potential for dimerization (pLDDT:
442 84.9, pTM: 0.798, ipTM: 0.783). C. Mature TIG-3(brown)/TIG-3(gray-beige) falls slightly
443 below (pLDDT: 68.8) the threshold for a confident structure prediction (pLDDT ≥ 70), and its
444 predicted ability to homodimerize is very low (ipTM: 0.288). Additionally, no confidently-
445 predicted (pTM: 0.522) interface residues exist between TIG-3 monomers.

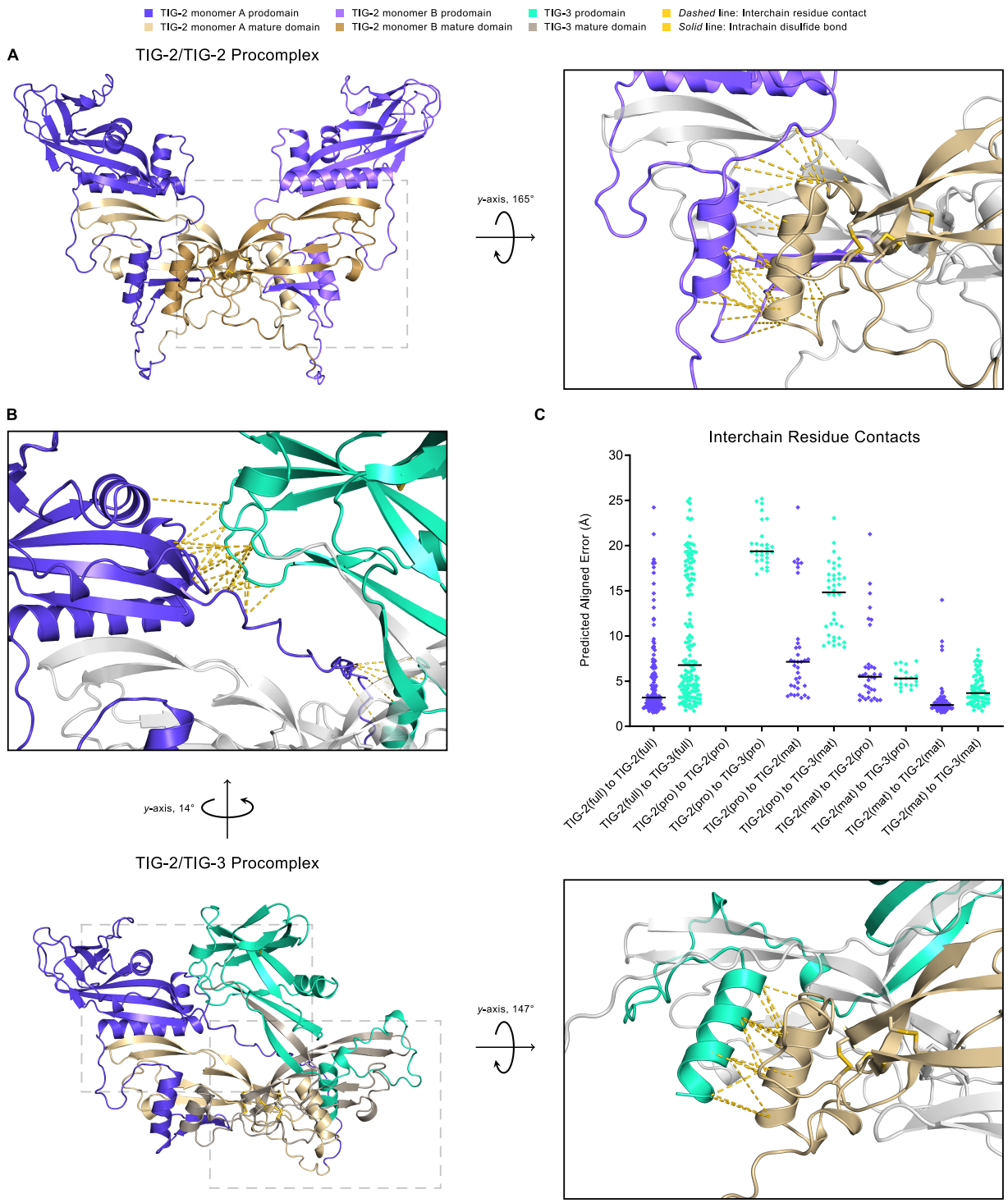

Figure 7. Structural Modeling of TIG-2/TIG-2 and TIG-2/TIG-3 Procomplexes Using AlphaFold2. A. The TIG-2/TIG-2 procomplex exhibits a symmetric open-arm conformation with monomer A in blue-violet (prodomain) and khaki (mature domain) and monomer B in light

450 blue-violet (prodomain) and dark khaki (mature domain). The right panel is the magnified and
451 rotated area defined by the gray dashed box in the left panel. Interchain residue contacts between
452 the mature domain (khaki) of pro-TIG-2 monomer A to the prodomain (light blue-violet) of pro-
453 TIG-2 monomer B are shown as gold *dashed* lines. As is true for the mature form, the TIG-3
454 homodimer procomplex (not shown) has significantly lower multimer metrics (pLDDT: 66.5,
455 pTM: 0.354, ipTM: 0.281) and thus a reduced predicted likelihood to homodimerize. B. The
456 TIG-2/TIG-3 procomplex adopts an asymmetric conformation, with pro-TIG-2 forming an open-
457 arm conformation and pro-TIG-3 (prodomain in green-cyan, mature domain in gray-beige)
458 presenting a crossed-arm conformation. Pro-TIG-2 contains no prodomain cysteines and hence is
459 not prodomain disulfide-linked to pro-TIG-3. The only two cysteines in the pro-TIG-3
460 prodomain are paired in an intra-prodomain 60-70 disulfide bond (*solid* gold line). The enlarged
461 upper panel corresponds to the upper-left dashed box following rotation to emphasize the
462 interchain residue contacts resulting from the prodomain of pro-TIG-3 (green-cyan) crossing
463 over to interact with the prodomain of pro-TIG-2 (blue-violet). Similarly to A, the right panel
464 corresponds to the lower-right gray dashed box and features interchain residue contacts between
465 the mature domain of pro-TIG-2 (khaki) and the prodomain of pro-TIG-3 (green-cyan). C. A
466 comparison of interchain residue contacts in TIG-2/TIG-2 (blue-violet diamonds) and TIG-
467 2/TIG-3 (green-cyan diamonds) procomplexes between combinatorial interacting monomer
468 regions (full: full-length, pro: prodomain, mat: mature domain) plotted with their predicted
469 aligned error value and column mean (black horizontal line). For example, the column TIG-
470 2(full) to TIG-3(full) contains all interchain residue contacts between pro-TIG-2 and pro-TIG-3.
471 Correspondingly, the column TIG-2(mat) to TIG-3(pro) includes all interchain residue contacts
472 between the mature domain of pro-TIG-2 to the prodomain of pro-TIG-3. The TIG-2/TIG-3

473 procomplex compares similarly to the TIG-2/TIG-2 procomplex with respect to full-length to
474 full-length (columns 1 and 2), mature domain to prodomain (columns 7 and 8), and mature
475 domain to mature domain contacts (columns 9 and 10).

476

477 **Discussion**

478 The multiplicity of TGF-β family ligands, receptors, and Smad signal transducers may support
479 the generation of diverse context-dependent outcomes through combinatorial interactions.
480 Biochemical and computational approaches are useful to identify the principles mediating the
481 potential protein-protein interactions between these components, but these approaches must be
482 complemented by functional in vivo analyses. The nematode *C. elegans* has five TGF-β ligands
483 and two characterized TGF-β family signaling pathways (Patterson and Padgett, 2000; MacNeill
484 *et al.*, 2009), providing a powerful in vivo system in which to study TGF-β ligand functions in
485 the context of the intact organism. Critically, TGF-β signaling mechanisms are conserved in this
486 organism. Here we demonstrate that all five TGF-β ligands play a role in the immune response
487 against bacterial pathogen. Furthermore, two ligand pairs consisting of a BMP subfamily and a
488 TGF-β/Activin subfamily member (TIG-2/TIG-3 and DBL-1/DAF-7) show evidence of acting
489 together in the response to gram-negative bacterium *P. luminescens.*

490

491 These studies were initiated with the well characterized BMP-like DBL-1 signaling pathway,
492 which is associated with significant roles in development and body size regulation but has also
493 been shown to play an important role in the immune response against both bacterial and fungal
494 pathogens (Mallo, 2002; Tenor and Aballay, 2008; Zugasti and Ewbank, 2009). Comparing the
495 response to the gram-negative bacteria *S. marcescens* and *P. luminescens*, we obtained evidence
496 implicating a level of specificity of ligand responses for particular bacteria. Although both BMP-
497 like ligands, DBL-1 and TIG-2, play a significant role in the response against *S. marcescens,*
498 TIG-2 has a more significant role than DBL-1 in the response against *P. luminescens*. These
499 results suggest that the function of DBL-1 in the immune response is not a general one-size-fits-

500 all response to bacterial pathogen but rather a more nuanced response with some level of
501 pathogen specificity. Furthermore, we show that DBL-1/BMP and TIG-2/BMP have additive
502 roles in the response to *P. luminescens,* suggesting that they trigger independent responses.
503 The orphan ligand UNC-129 shows moderate and variably significant changes in survival on *P.*
504 *luminescens,* suggesting a minor or modulatory role. The TGF-β/Activin-like ligands DAF-7 and
505 TIG-3 demonstrated consistently significant reduced survival patterns on *P. luminescens*
506 suggesting involvement of these ligands in the response to this bacterial pathogen. qRT-PCR
507 analysis of TGF-β ligand expression shows that with 24-hour exposure to bacterial infection,
508 expression levels of the ligands do not significantly change from control conditions. A
509 *dbl-1p*::GFP transcriptional reporter validates these results for *dbl-1.* Taken together, we
510 conclude that all five of the TGF-β ligands play a role in the immune response, but not at the
511 level of transcriptional induction.
512
513 Analysis of the survival patterns of double mutant animals produced results indicating
514 interactions between multiple TGF-β family ligands. Interestingly, the interactions between pairs
515 of BMP-like and TGF-β/Activin-like ligands suggest cooperative interaction in a common
516 pathway. Specifically, the *tig-3;tig-2* double mutant survival pattern is no more severe than
517 either single mutant alone. Similarly, the *daf-7;dbl-1* double mutant survival is indistinguishable
518 from that of *dbl-1* single mutants. Of these pairs, TIG-2 and TIG-3 play a more major role in the
519 response to *P. luminescens.* We therefore used computational modeling to determine whether
520 these ligands could feasibly function as a heterodimer. Using ColabFold, we demonstrated that a
521 TIG-2/TIG-3 heterodimer is better supported than the TIG-3 homodimer. Furthermore, *tig-2* and
522 *tig-3* expression overlaps in neurons such as AFD and M2. These neurons are located adjacent to
523 the pharynx. We have shown that SMA-3/Smad is required in pharyngeal muscle for survival on

524 bacterial pathogens (Ciccarelli *et al.,* 2023), so TIG-2 and TIG-3 are produced in a location
525 appropriate for signaling to SMA-3/Smad in the pharynx.
526
527 We also identify the canonical BMP-like pathway as required for response to *P. luminescens,*
528 including the Type I receptor (SMA-6), the R-Smads (SMA-2 and SMA-3) and Co-Smad
529 (SMA-4). In contrast, TGF-β/Activin pathway components have minimal effects. Unlike *dbl-1*
530 mutants*, tig-2* and *tig-3* mutants have very similar survival phenotypes to *sma-3* mutants.
531 Furthermore, *tig-2, tig-3,* and *sma-3* mutants share a pharyngeal pumping defect that is not seen
532 in *dbl-1* mutants. These similarities provide evidence that TIG-2 and TIG-3 signal through the
533 canonical BMP signaling pathway consisting of SMA-6 Type I receptor, and SMA-2, SMA-3,
534 and SMA-4 Smads in the context of bacterial pathogen survival. There is precedence for
535 TGF-β/Activin ligands signaling through BMP-like signaling pathways in vertebrates. For
536 example, in endothelial cells, TGF-β can phosphorylate presumptive BMP Smads Smad1/5
537 through interaction with type I receptor ALK1 rather than ALK5 (Lebrin *et al.,* 2005).
538 Furthermore, the BMP receptor ALK2 (ACVR1) can be activated by Activin to phosphorylate
539 Smad1/5, and this activity is increased by pathogenic FOP mutations (Ramachandran *et al.,*
540 2021). However, cooperative action between a BMP and TGF-β/Activin ligand, including
541 potential cross-subfamily heterodimers, has not yet been described in vertebrates to our
542 knowledge, and warrants further consideration.
543
544 Interestingly, nonredundant roles for TIG-2, TIG-3, and UNC-129 have recently been identified
545 in neuronal guidance in *C. elegans* (Baltaci *et al.,* 2022). In neuronal guidance, TIG-3/UNC-129
546 heterodimers are implicated, with TIG-2 being released from a different tissue. In this context,

547 the ligands depend on the BMP signaling components SMA-6 Type I Receptor and SMA-2,
548 SMA-3, and SMA-4 Smads. Relatedly, in Drosophila, three Activin ligands are required
549 nonredundantly to regulate photoreceptor identity through the canonical Activin signaling
550 components (Wells *et al.*, 2017). In addition to heterodimers, nonredundant functions of TGF-β
551 ligands can be explained by a receptor clustering mechanism that generates higher-order
552 signaling complexes (Ramachandran *et al.*, 2018). Our system provides a platform for studying
553 the functional interactions between multiple TGF-β ligands. Cooperativity between BMP and
554 TGF-β/Activin subfamily members may provide a mechanism for distinguishing the
555 developmental and homeostatic functions of these ligands from an acute response such as the
556 innate immune response to bacterial pathogens.
557

558 **Acknowledgements**

559 This work was funded by R15GM112147 to CSD (National Institutes of Health/NIGMS). Some
560 strains were provided by the Caenorhabditis Genetics Center, which is supported by the National
561 Institute of Health – Office of Research Infrastructure Programs (P40 OD010440). We are
562 grateful to the lab of Roger Pocock for sharing double and triple mutants of TGF-β ligand genes.
563 We thank Jan Christian for helpful comments on the manuscript. This work was carried out in
564 partial fulfillment of the requirements for the Ph.D. degree from the Graduate Center of City
565 University of New York (EJC).
566

567 **References**

568 Attisano L, Wrana JL. 1996. Signal transduction by members of the transforming growth factor-
569 beta superfamily. *Cytokine Growth Factor Rev* **7**:327–339. doi:10.1016/s1359-
570 6101(96)00042-1

571 Aykul S, Martinez-Hackert E. 2016. Transforming Growth Factor-β Family Ligands Can
572 Function as Antagonists by Competing for Type II Receptor Binding. *J Biol Chem*
573 **291**:10792–10804. doi:10.1074/jbc.M115.713487

574 Baltaci O, Pedersen ME, Sherry T, Handley A, Snieckute G, Cao W, Haas M, Archer S, Pocock
575 R. 2022. Atypical TGF-β signaling controls neuronal guidance in Caenorhabditis elegans.
576 *iScience* **25**:103791. doi:10.1016/j.isci.2022.103791

577 Blobe GC, Schiemann WP, Lodish HF. 2000. Role of transforming growth factor beta in human
578 disease. *N Engl J Med* **342**:1350–1358. doi:10.1056/NEJM200005043421807

579 Ciccarelli EJ, Bendelstein M, Savage-Dunn C. 2023. BMP signaling to pharyngeal muscle in the
580 *C. elegans* immune response to bacterial pathogen regulates anti-microbial peptide
581 expression and pharyngeal pumping. doi: 10.1101/2023.03.06.531324

582 Derynck R, Akhurst RJ, Balmain A. 2001. TGF-beta signaling in tumor suppression and cancer
583 progression. *Nat Genet* **29**:117–129. doi:10.1038/ng1001-117

584 Derynck R, Zhang Y, Feng XH. 1998. Smads: transcriptional activators of TGF-beta responses.
585 *Cell* **95**:737–740. doi:10.1016/s0092-8674(00)81696-7

586 Estevez M, Attisano L, Wrana JL, Albert PS, Massagué J, Riddle DL. 1993. The daf-4 gene
587 encodes a bone morphogenetic protein receptor controlling C. elegans dauer larva
588 development. *Nature* **365**:644–649. doi:10.1038/365644a0

589 Gray AM, Mason AJ. 1990. Requirment for activin A and transforming growth factor-β1 pro-
590 regions in homodimer assembly. *Science.* **247**:1328–1330. doi:10.1126/science.2315700

591 Georgi LL, Albert PS, Riddle DL. 1990. Daf-1, a C. elegans gene controlling dauer larva
592 development, encodes a novel receptor protein kinase. *Cell* **61**:635–645. doi:10.1016/0092-
593 8674(90)90475-t

594 Herpin A, Lelong C, Favrel P. 2004. Transforming growth factor-beta-related proteins: an
595 ancestral and widespread superfamily of cytokines in metazoans. *Dev Comp Immunol*
596 **28**:461–485. doi:10.1016/j.dci.2003.09.007

597 Hinck AP, Mueller TD, Springer TA. 2016. Structural biology and evolution of the TGF-β
598 family. *Cold Spring Harb Perspect Biol*. **8**:a022103. doi:10.1101/cshperspect.a022103

599 Hoffmann JA, Kafatos FC, Janeway CA, Ezekowitz RA. 1999. Phylogenetic perspectives in
600 innate immunity. *Science* **284**:1313–1318. doi:10.1126/science.284.5418.1313

601 Huminiecki L, Goldovsky L, Freilich S, Moustakas A, Ouzounis C, Heldin C-H. 2009.
602 Emergence, development and diversification of the TGF-βsignalling pathway within the
603 animal kingdom. *BMC Evolutionary Biology* **9**:28. doi:10.1186/1471-2148-9-28

604 Irazoqui JE, Ng A, Xavier RJ, Ausubel FM. 2008. Role for beta-catenin and HOX transcription
605 factors in Caenorhabditis elegans and mammalian host epithelial-pathogen interactions.
606 *Proc Natl Acad Sci U S A* **105**:17469–17474. doi:10.1073/pnas.0809527105

607 Jumper J, Evans R, Pritzel A, Green T, Figurnov M, Ronneberger O, Tunyasuvunakool K, Bates

608 R, Žídek A, Potapenko A, Bridgland A, Meyer C, Kohl SAA, Ballard AJ, Cowie A,
609 Romera-Paredes B, Nikolov S, Jain R, Adler J, Back T, Petersen S, Reiman D, Clancy E,
610 Zielinski M, Steinegger M, Pacholska M, Berghammer T, Bodenstein S, Silver D, Vinyals
611 O, Senior AW, Kavukcuoglu K, Kohli P, Hassabis D. 2021. Highly accurate protein
612 structure prediction with AlphaFold. *Nature* **596**:583–589. doi:10.1038/s41586-021-03819-
613 2

614 Kim DH, Feinbaum R, Alloing G, Emerson FE, Garsin DA, Inoue H, Tanaka-Hino M, Hisamoto
615 N, Matsumoto K, Tan M-W, Ausubel FM. 2002. A conserved p38 MAP kinase pathway in
616 Caenorhabditis elegans innate immunity. *Science* **297**:623–626.
617 doi:10.1126/science.1073759

618 Kim H-S, Neugebauer J, McKnite A, Tilak A, Christian JL. 2019. BMP7 functions
619 predominantly as a heterodimer with BMP2 or BMP4 during mammalian embryogenesis.
620 *eLife* **8**:e48872. doi:10.7554/eLife.48872

621 Krishna S, Maduzia LL, Padgett RW. 1999. Specificity of TGFbeta signaling is conferred by
622 distinct type I receptors and their associated SMAD proteins in Caenorhabditis elegans.
623 *Development* **126**:251–260. doi:10.1242/dev.126.2.251

624 Lebrin F, Deckers M, Bertolino P, Ten Dijke P. 2005. TGF-beta receptor function in the
625 edothelium. Cardiovasc Res **65**:599-608. doi: 10.1016/j.cardiores.2004.10.036.

626 Li M, Wan Y, Sanjabi S, Robertson A-K, Flavell R. 2006. Transforming growth factor-
627 regulation of immune responses. *Annual Review of Immunology* **24:**99-146. doi:
628 10.1146/annurev.immunol.24.021605.090737

629 Little SC, Mullins MC. 2009. Bone morphogenetic protein heterodimers assemble heteromeric
630 type I receptor complexes to pattern the dorsoventral axis. *Nat Cell Biol* **11**:637–643.
631 doi:10.1038/ncb1870

632 MacNeil LT, Hardy WR, Pawson T, Wrana JL, Culotti JG. 2009. UNC-129 regulates the balance
633 between UNC-40 dependent and independent UNC-5 signaling pathways. *Nat Neurosci*
634 **12**:150–155. doi:10.1038/nn.2256

635 Mallo GV, Kurz CL, Couillault C, Pujol N, Granjeaud S, Kohara Y, Ewbank JJ. 2002. Inducible
636 antibacterial defense system in C. elegans. *Curr Biol* **12**:1209–1214. doi:10.1016/s0960-
637 9822(02)00928-4

638 Massagué J. 2012. TGFβ signalling in context. *Nat Rev Mol Cell Biol* **13**:616–630.
639 doi:10.1038/nrm3434

640 Massagué J. 2008. TGFbeta in Cancer. *Cell* **134**:215–230. doi:10.1016/j.cell.2008.07.001

641 Massagué J. 1998. TGF-beta signal transduction. *Annu Rev Biochem* **67**:753–791.
642 doi:10.1146/annurev.biochem.67.1.753

643 Massagué J, Chen YG. 2000. Controlling TGF-beta signaling. *Genes Dev* **14**:627–644.

644 Medzhitov R, Janeway CA. 1998. Innate immune recognition and control of adaptive immune
645 responses. *Semin Immunol* **10**:351–353. doi:10.1006/smim.1998.0136

646 Millet ACM, Ewbank JJ. 2004. Immunity in Caenorhabditis elegans. *Curr Opin Immunol* **16**:4–
647 9. doi:10.1016/j.coi.2003.11.005

648 Mirdita M, Schütze K, Moriwaki Y, Heo L, Ovchinnikov S, Steinegger M. 2022. ColabFold:

649 making protein folding accessible to all. *Nat Methods* **19**:679–682. doi:10.1038/s41592-
650 022-01488-1

651 Morita K, Flemming AJ, Sugihara Y, Mochii M, Suzuki Y, Yoshida S, Wood WB, Kohara Y,
652 Leroi AM, Ueno N. 2002. A Caenorhabditis elegans TGF-β, DBL-1, controls the expression
653 of LON-1, a PR-related protein, that regulates polyploidization and body length. *EMBO J*
654 **21**:1063–1073. doi:10.1093/emboj/21.5.1063

655 Mottershead DG, Sugimura S, Al-Musawi SL, Li JJ, Richani D, White MA, Martin GA, Trotta
656 AP, Ritter LJ, Shi J, Mueller TD, Harrison CA, Gilchrist RB. 2015. Cumulin, an oocyte-
657 secreted heterodimer of the transforming growth factor- β family, is a potent activator of
658 granulosa cells and improves oocyte quality. *J Biol Chem* **290**:24007-20.
659 doi:10.1074/jbc.M115.671487

660 Neugebauer JM, Kwon S, Kim HS, Donley N, Tilak A, Sopory S, Christian JL. 2015. The
661 prodomain of BMP4 is necessary and sufficient to generate stable BMP4/7 heterodimers
662 with enhanced bioactivity in vivo. *Proc Natl Acad Sci USA* **112**:E2307-16. doi:
663 10.1073/pnas.1501449112.

664 Partridge FA, Gravato-Nobre MJ, Hodgkin J. 2010. Signal transduction pathways that function
665 in both development and innate immunity. *Developmental Dynamics* **239**:1330–1336.
666 doi:10.1002/dvdy.22232

667 Patterson GI, Padgett RW. 2000. TGF beta-related pathways. Roles in Caenorhabditis elegans
668 development. *Trends Genet* **16**:27–33. doi:10.1016/s0168-9525(99)01916-2

669 Peng J, Li Q, Wigglesworth K, Rangarajan A, Kattamuri C, Peterson RT, Eppig JJ, Thompson
670 TB, Matzuk MM. 2013. Growth differentiation factor 9: bone morphogenetic protein 15

671 heterodimers are potent regulators of ovarian functions. *Proc. Natl. Acad. Sci. U.S.A.*
672 **110**:E777-E785. doi:10.1073/pnas.1218020110

673 Pohlers D, Brenmoehl J, Löffler I, Müller CK, Leipner C, Schultze-Mosgau S, Stallmach A,
674 Kinne RW, Wolf G. 2009. TGF-beta and fibrosis in different organs - molecular pathway
675 imprints. *Biochim Biophys Acta* **1792**:746–756. doi:10.1016/j.bbadis.2009.06.004

676 Principe DR, Doll JA, Bauer J, Jung B, Munshi HG, Bartholin L, Pasche B, Lee C, Grippo PJ.
677 2014. TGF-β: duality of function between tumor prevention and carcinogenesis. *J Natl*
678 *Cancer Inst* **106**:djt369. doi:10.1093/jnci/djt369

679 Ramachandran A, Vizán P, Das D, Chakravarty P, Vogt J, Rogers KW, Müller P, Hinck AP,
680 Sapkota GP, Hill CS. 2018. TGF-β uses a novel mode of receptor activation to
681 phosphorylate SMAD1/5 and induce epithelial-to-mesenchymal transition. *eLife* **7**:e31756.
682 doi:10.7554/eLife.31756

683 Ramachandran A, Mehić M, Wasim L, Malinova D, Gori I, Blaszczyk BK, Carvalho DM, Shore
684 EM, Jones C, Hyvönen M, Tolar P, Hill CS. 2021. Pathogenic ACVR1^{R206H} activation by
685 activin A-induced receptor clustering and autophosphorylation. *EMBO J* **40**:e106317. doi:
686 10.15252/embj.2020106317

687 Savage C, Das P, Finelli AL, Townsend SR, Sun CY, Baird SE, Padgett RW. 1996.
688 Caenorhabditis elegans genes sma-2, sma-3, and sma-4 define a conserved family of
689 transforming growth factor beta pathway components. *Proc Natl Acad Sci U S A* **93**:790–
690 794. doi:10.1073/pnas.93.2.790

691 Savage-Dunn C, Padgett RW. 2017. The TGF-β Family in Caenorhabditis elegans. *Cold Spring*
692 *Harb Perspect Biol* **9**:a022178. doi:10.1101/cshperspect.a022178

693 Schulenburg H, Kurz CL, Ewbank JJ. 2004. Evolution of the innate immune system: the worm
694 perspective. *Immunol Rev* **198**:36–58. doi:10.1111/j.0105-2896.2004.0125.x

695 Shimmi O, Umulis D, Othmer H, O'Connor MB. 2005. Facilitated transport of a Dpp/Scw
696 heterodimer by Sog/Tsg leads to robust patterning of the Drosophila blastoderm embryo.
697 *Cell* **120**:873–886. doi:10.1016/j.cell.2005.02.009

698 Silberstein GB, Daniel CW. 1987. Reversible inhibition of mammary gland growth by
699 transforming growth factor-beta. *Science* **237**:291–293. doi:10.1126/science.3474783

700 Suzuki Y, Yandell MD, Roy PJ, Krishna S, Savage-Dunn C, Ross RM, Padgett RW, Wood WB.
701 1999. A BMP homolog acts as a dose-dependent regulator of body size and male tail
702 patterning in Caenorhabditis elegans. *Development* **126**:241–250.
703 doi:10.1242/dev.126.2.241

704 Tenor JL, Aballay A. 2008. A conserved Toll-like receptor is required for Caenorhabditis
705 elegans innate immunity. *EMBO Rep* **9**:103–109. doi:10.1038/sj.embor.7401104

706 Tillet E, Ouarné M, Desroches-Castan A, Mallet C, Subileau M, Didier R, Lioutsko A, Belthier
707 G, Feige J-J, Bailly S. 2018. A heterodimer formed by bone morphogenetic protein 9
708 (BMP9) and BMP10 provides most BMP biological activity in plasma. *J Biol Chem*
709 **293**:10963–10974. doi:10.1074/jbc.RA118.002968

710 Valera E, Isaacs MJ, Kawakami Y, Izpisua Belmonte JC, Choe S. 2010. BMP2/6 heterodimer is

711 more effective than BMP-2 or BMP-6 homodimers as inductor of differentiation of
712 human embryonic stem cells. *PLoS One*. **5**:e11167. doi:10.1371/journal.pone.0011167

713 Walton KL, Makanji Y, Wilce MC, Chan KL, Robertson DM, Harrison CA. 2009. A common
714 biosynthetic pathway governs the dimerization and secretion of inhibin and related
715 transforming growth factor b (TGFb) ligands. *J Biol Chem* **284**: 9311–9320.
716 doi:10.1074/jbc.M808763200

717 Wang J, Tokarz R, Savage-Dunn C. 2002. The expression of TGFbeta signal transducers in the
718 hypodermis regulates body size in C. elegans. *Development* **129**:4989–4998.
719 doi:10.1242/dev.129.21.4989

720 Wells BS, Pistillo D, Barnhart E, Desplan C. 2017. Parallel Activin and BMP signaling
721 coordinates R7/R8 photoreceptor subtype pairing in the stochastic Drosophila retina. *eLife*
722 **6**:e25301. doi:10.7554/eLife.25301

723 Wisotzkey RG, Newfeld SJ. 2020. TGF-β prodomain alignments reveal unexpected cysteine
724 conservation consistent with phylogenetic predictions of cross-subfamily
725 heterodimerization. *Genetics* **214**:447-465. doi: 10.1534/genetics.119.302255

726 Wrana JL. 2013. Signaling by the TGF-β Superfamily. *Cold Spring Harb Perspect Biol*
727 **5**:a011197. doi:10.1101/cshperspect.a011197

728 Wrana JL, Attisano L, Wieser R, Ventura F, Massagué J. 1994. Mechanism of activation of the
729 TGF-β receptor. *Nature* **370**:341–347. doi:10.1038/370341a0

730 Yin J, Madaan U, Park A, Aftab N, Savage-Dunn C. 2015. Multiple cis elements and GATA
731 factors regulate a cuticle collagen gene in *Caenorhabditis elegans*. *Genesis* **53**:278-284. doi:
732 10.1002/dvg.22847

733 Yoshida S, Morita K, Mochii M, Ueno N. 2001. Hypodermal expression of Caenorhabditis
734 elegans TGF-beta type I receptor SMA-6 is essential for the growth and maintenance of
735 body length. *Dev Biol* **240**:32–45. doi:10.1006/dbio.2001.0443

736 Zamarron BF, Chen W. 2011. Dual roles of immune cells and their factors in cancer
737 development and progression. *Int J Biol Sci* **7**:651–658. doi:10.7150/ijbs.7.651

738 Zhu J, Braun EL, Kohno S, Antenos M, Xu EY, Cook RW, Lin SJ, Moore BC, Guillette Jr LJ,
739 Jardetzky TS, Woodruff TK. 2010. Phylogenomic analyses reveal the evolutionary origin
740 of the inhibin α-subunit, a unique TGFβ superfamily antagonist. *PLoS ONE* **5**: e9457.
741 doi:10.1371/journal.pone.0009457

742

743 **Supplemental Figures**

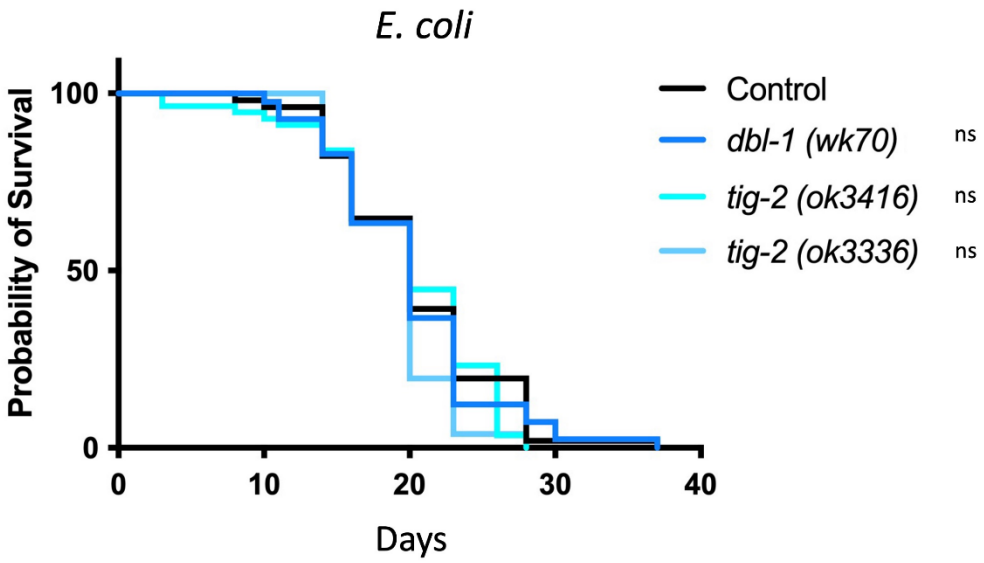

744

745 Figure S1. Lifespan analysis of *dbl-1(wk70), tig-2(ok3416),* and *tig-2(ok3336)* on nonpathogenic

746 *E. coli* strain DA837. n values: Control (51), *dbl-1* (41), *tig-2* (56), *tig-2* (51).

747

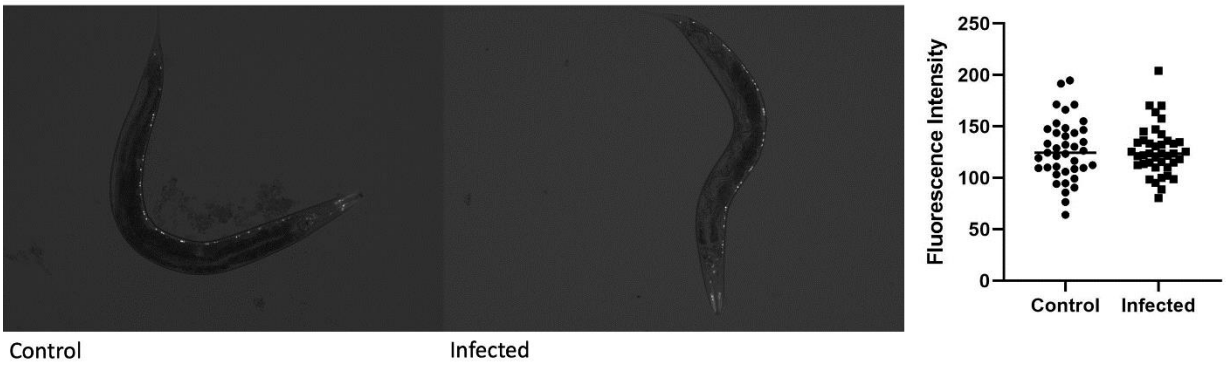

748

749 Figure S2. Reporter imaging of *dbl-1p::*GFP transcriptional reporter on control *E.* coli and 24-

750 hour infection on *P. luminescens* bacteria. No significance.

751

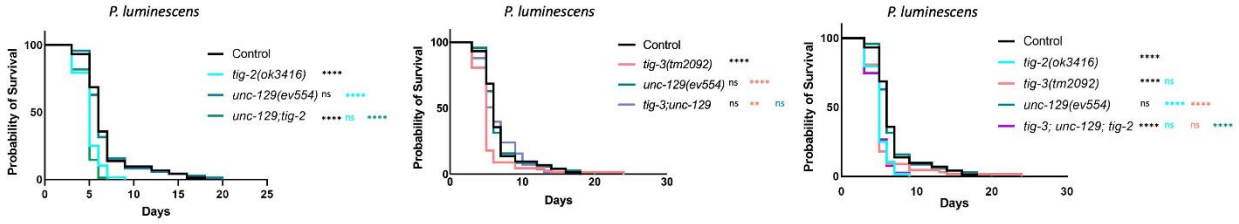

Figure S3. Survival analysis of *unc-129(ev554);tig-2(3416), unc-129(ev554);tig-3(tm2092),* and *tig-3(tm2092);unc-129(ev554);tig-2(ok3416)*. n values: Control (73), *tig-2* (68), *unc-129* (70), *unc-129;tig-2* (83), *tig-3* (67), *tig-3;unc-129* (83), *tig-3;unc-129;tig-2* (79). Statistical analysis for survival analyses done using Log-rank (Mantel-Cox) Test.

```
TIG-3.B          ----------NAPNFDVMVFQP-NTVTAGTSDCVGCCVIPFYVNFTEIGWNDWILSPPGF       49
INHA_HUMAN       ------STPLMSWPWSPSALRLLQRPPEEPAAHANCHRVALNISFQELGWERWIVYPPSF       54
GDF9_HUMAN       -GQETVSSELKK-PLGPASFNLSEYFRQFLLPQNECELHDFRLSFSQLKWDNWIVAPHRY       58
BMP15_HUMAN      -QADGISAEVT-----------ASSSKHSGPENNQCSLHPFQISFRQLGWDHWIIAPPFY       48
INHBA_HUMAN      -------------------------GLECDGKVNICCKKQFFVSFKDIGWNDWIIAPSGY       35
TIG-2            ---------------------SESAYFEKPNENERCQRKGLYVDFDILGWKQWVIAPEGF       39
BMP2_HUMAN       -----------------------QAKHKQRKRLKSSCKRHPLYVDFSDVGWNDWIVAPPGY       38
DBL-1            SAQTGNSERKNR--------KKGRKHHNTEAESNLCRRTDFYVDFDDLNWQDWIMAPKGY       52
                                                   *    : :.*  : *. *:: *  :

TIG-3.B          YANVCSDTVC--------ST-----ESDEVYQFMKAAISDLPEPKCA--PNYYGSVDMIV       94
INHA_HUMAN       IFHYCHGGCGLHIPPNLSLP----VPGAPPTPAQPYSLLPGAQPCCAALPGTMRPLHVRT      110
GDF9_HUMAN       NPRYCKGDCPRAVGHRYGSP----VHTMVQNIIYEKLDSSVPRPSCV--PAKYSPLSVLT      112
BMP15_HUMAN      TPNYCKGTCLRVLRDGLNSP----NHAIIQNLINQLVDQSVPRPSCV--PYKYVPISVLM      102
INHBA_HUMAN      HANYCEGECPSHIAGTSGSSLSFHSTVINHYRMRGHSPFANLKSCCV--PTKLRPMSMLY       93
TIG-2            SAFYCSGDCSAPFSKEMNAT----SHAIVQSTLHRVRPNSTTPAKCA--PSSLGSYKILF       93
BMP2_HUMAN       HAFYCHGECPFPLADHLNST----NHAIVQTLVNSVN-SKIPKACCV--PTELSAISMLY       91
DBL-1            DAYQCQGSCPNPMPAQLNAT----NHAIIQSLLHSLRPDEVPPPCCV--PTETSPLSILY      106
                     * .                                     *   *       :

TIG-3.B          ALS-PRDIRKTRVHGLRALSCSCT      117
INHA_HUMAN       TSDGGYSFKYETVPNLLTQHCACI      134
GDF9_HUMAN       IEP-DGSIAYKEYEDMIATKCTCR      135
BMP15_HUMAN      IEA-NGSILYKEYEGMIAESCTCR      125
INHBA_HUMAN      YDD-GQNIIKKDIQNMIVEECGCS      116
TIG-2            VDQ-NKQVQIKRYRDMVVDECGCH      116
BMP2_HUMAN       LDE-NEKVVLKNYQDMVVEGCGCR      114
DBL-1            MDV-DKVIVIREYADMRVESCGCR      129
                        .      .: .  * *
```

Figure S4. Multiple Sequence Alignment using Clustal Omega of Mature TIG-3, Inhibin α, GDF-9, BMP-15, Inhibin βA, TIG-2, BMP-2, and DBL-1. The conventional dimerization cysteine is highlighted in gold and replaced by lysine (yellow-green) in TIG-2 and TIG-3 and by serine (cyan) in GDF-9 and BMP-15. Consensus symbols (asterisk, colon, period) are defined according to standard Clustal Omega notation.

A

```
     >TIG-2
  1  MLFEFSILLGFLVPRGDSKGIYFVEERNGKTYTQPLTGQATDKIGEQIRE
 51  LFNIDINPNGPAVKANNYVSTYMKRLYKQLENYEHGENHNEEEVNAWLSA
101  DRIVSHMAQEVSHRLDDGSYSIRFAKEHVPAKEGQSIVRAQLRIHIQGIV
151  SPVFFYIEDTNLPGDTVLVSSDDPTVVTDVTTMVDRWSHLQLSTLPIVTA
201  RASTNDELKIEAFLVIALKDEDAGPPKKRSRRSASTTPISAPPMRQKVKR
251  SESAYFEKPNENERCQRKGLYVDFDILGWKQWVIAPEGFSAFYCSGDCSA
301  PFSKEMNATSHAIVQSTLHRVRPNSTTPAKCAPSSLGSYKILFVDQNKQV
351  QIKRYRDMVVDECGCH
```

```
     >TIG-3, isoform B
  1  MHFFTRFHYCFVITIISINASSLSIERQKRQLLSALNLSSRPPLIHQAPV
 51  IPDSMSTSRKHDLYGGVLDKITLEPNRKSWTCLTPESLVKDCFQYSINSI
101  NHEILSASLIIDPKDTNISIVVYEVDELFGELQYVDRFEIRETLDKYHFD
151  ISHLFHKWMKQKSSDKMIKIEITNSNTQNVINALSVLRNAPNFDVMVFQP
201  NTVTAGTSDCVGCCVIPFYVNFTEIGWNDWILSPPGFYANVCSDTVCSTE
251  SDEVYQFMKAAISDLPEPKCAPNYYGSVDMIVALSPRDIRKTRVHGLRAL
301  SCSCT
```

B

Protein	Subfamily[a]	Species	Uniprot Entry	Signal Sequence[b]	(Prodomain ⊃	Cleavage Site)	Mature Domain
TIG-2	BMP	*C. elegans*	O16273	MLFEFSILLGFLVPRGDS	…PMRQ	KVKR[c]	SESA…
TIG-3	Activin	*C. elegans*	A0A8S4QGI4	MHFFTRFHYCFVITIISINASS	…INAL	SVLR[a]	NAPN…
BMP-2	BMP	*H. sapiens*	P12643	MVAGTRCLLALLLPQVLLGGAAG	…PLHK	REKR[d]	QAKH…
BMP-6	BMP	*H. sapiens*	P22004	MPGLGRRAQWLCWWWGLLCS	…RQQS	R[d]	NRST…
BMP-15	BMP	*H. sapiens*	O95972	MVLLSILRILFLCELVLFMEHRAQM	…ESLL	RRTR[d]	QADG…
GDF-9	BMP	*H. sapiens*	O60383	MARPNKFLLWFCCFAWLCFPISLG	…SSHH	RHRR[d]	GQET…
Inh-βA	Activin	*H. sapiens*	P08476	MPLLWLRGFLLASCWIIVRS	…HPHR	RRRR[d]	GLEC…
Inh-βB	Activin	*H. sapiens*	P09529	MDGLPGRALGAACLLLLAAGWLGPEAW	…HRIR	KR[d]	GLEC…
Inh-α	TGF-β	*H. sapiens*	P05111	MVLHLLLFLLLTPQGGHS	…SGGE	RARR[d]	STPL…

a. Source: Newfeld and Wisotzkey, 2020
b. Source: SignalP 6.0
c. Source: Manual sequence analysis
d. Source: Hinck et al., 2016

Figure S5. Structural Modeling Sequence Data. A. Annotated TIG-2 and TIG-3 isoform B amino acid sequences. The signal sequence is underlined, and the cleavage site is in boldface. The prodomain includes the cleavage site, which separates the prodomain from the mature ligand. Cysteine residues participating in intrachain disulfide bonds are highlighted in gold. The lysine residue that replaces the dimerization cysteine is colored yellow-green. B. Subfamily, species, Uniprot entry, signal sequence, and cleavage site for modeled TGF-β family members.

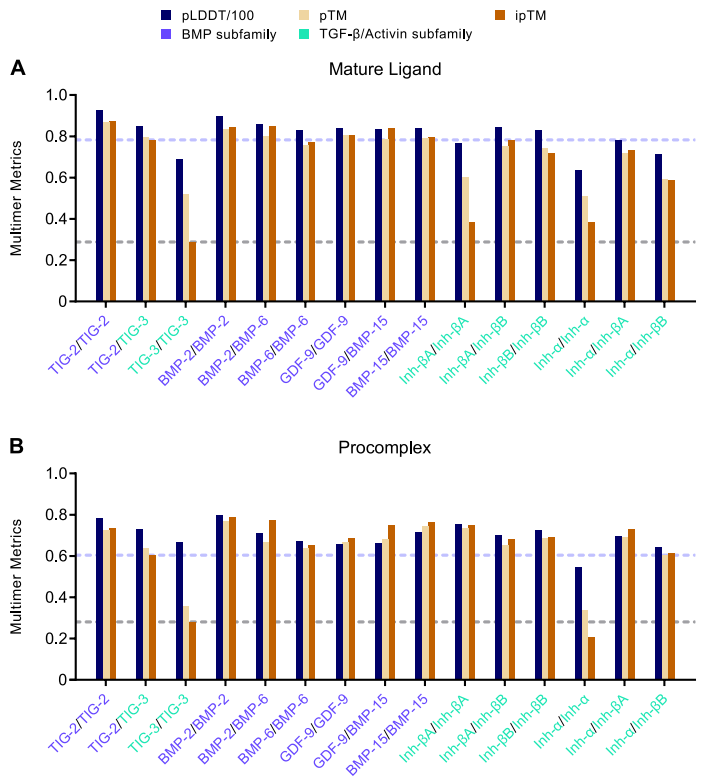

Figure S6. Benchmarking AlphaFold2 Structure Predictions against Experimentally Tested TGF-β Family Complexes. TIG-2 and TIG-3 structure predictions benchmarked against predictions for experimentally reported dimers (Valera *et al.*, 2010; Peng *et al.*, 2013; Mottershead *et al.*, 2015; Walton *et al.*, 2009) and the non-homodimeric inhibin α-subunit complex (Zhu *et al.*, 2010). Average pLDDT divided by 100 (navy), pTM (khaki), and ipTM (amber) metrics are grouped for each complex. Lavender and gray dashed lines correspond to TIG-2/TIG-3 and TIG-3/TIG-3 ipTM scores, respectively. Monomers are color-coded according to TGF-β subfamily, with BMP in blue-violet and TGF-β/Activin in green-cyan. Both mature and procomplexes of the TIG-2 homodimer and TIG-2/TIG-3 heterodimer converge with known dimers. In contrast, the mature and pro-forms of the TIG-3 homodimer markedly diverge with inhibin α that does not homodimerize. Mature activin A, the inhibin βA homodimer, groups with mature inhibin α despite the established ability of inhibin βA to homodimerize. Activin A

786 procomplex, however, expectedly groups with the reported dimers. The mature and pro results
787 together support the necessity of prodomain-mediated dimerization for activin A, as previously
788 shown (Gray and Mason, 1990). Reported non-disulfide-linked mature dimers include GDF-
789 9/GDF-9, GDF-9/BMP-15, and BMP-15/BMP-15. Procomplex multimer metrics are observably
790 lower (except for pTM and iPTM scores for activin A and inhibin B) than the equivalent mature
791 form.
792
793